ΔNp63α-mediated regulation of tumor-associated genes and pathways in hepatocellular carcinoma progression

XIAOWEN LIN[1*], ANGHUI PENG[1*], MIN ZHANG[2] and XINYANG YU[1]

[1]Guangdong Provincial Key Laboratory of Tumor Interventional Diagnosis and Treatment, Zhuhai Institute of Translational Medicine, Zhuhai People's Hospital (The Affiliated Hospital of Beijing Institute of Technology, Zhuhai Clinical Medical College of Jinan University), Zhuhai, Guangdong 519000, P.R. China; [2]Department of Pharmacy, Shandong Provincial Maternal and Child Health Care Hospital Affiliated to Qingdao University, Jinan, Shandong 250014, P.R. China

Received March 19, 2026; Accepted September 8, 2026

DOI: 10.3892/mmr.2026.14040

Abstract. ΔNp63α is key in cellular development and epithelial tumors; however, its role in hepatocellular carcinoma (HCC) remains unclear. In the present study, the oncogenic role and molecular functions of ΔNp63α in HCC were investigated. Analysis of The Cancer Genome Atlas revealed an association between p63 expression and patient survival. ΔNp63α overexpression in SNU387 cells notably enhanced cell proliferation and migration, supporting its role in promoting aggressive HCC phenotypes. Transcriptome analysis revealed extensive ΔNp63α-associated transcriptional changes, with differentially expressed genes enriched in tumor-associated processes, including 'Wnt signaling pathway', 'Notch signaling pathway', 'cell adhesion molecules' and 'extracellular matrix organization'. Chromatin immunoprecipitation sequencing revealed widespread ΔNp63α binding in promoter-proximal and -distal regulatory regions, suggesting potential involvement in transcriptional regulation through both proximal and distal genomic elements. ΔNp63α upregulation was also associated with increased CCCTC-binding factor (CTCF) occupancy near the promoters of tumor-associated genes and these gained CTCF sites were enriched for p63 motifs. Collectively, the present findings identified ΔNp63α as an oncogenic regulator of HCC and suggest that it may regulate tumor-associated gene programs through coordinated proximal and distal chromatin regulatory mechanisms.

Correspondence to: Dr Xinyang Yu, Guangdong Provincial Key Laboratory of Tumor Interventional Diagnosis and Treatment, Zhuhai Institute of Translational Medicine, Zhuhai People's Hospital (The Affiliated Hospital of Beijing Institute of Technology, Zhuhai Clinical Medical College of Jinan University), 79 Kangning Road, Zhuhai, Guangdong 519000, P.R. China
E-mail: xinyang910@gmail.com

*Contributed equally

Key words: ΔNp63α, hepatocellular carcinoma, gene regulation, CCCTC-binding factor

Introduction

Liver cancer remains a notable global health challenge, being the sixth most common malignancy worldwide, with increasing annual incidence and mortality rates (1). According to global cancer statistics for 2022, there were >860,000 new liver cancer cases and nearly 760,000 liver cancer-associated mortalities reported annually (2). Liver cancer encompasses three distinct pathological subtypes: Hepatocellular carcinoma (HCC), intrahepatic cholangiocarcinoma and mixed hepatocellular-cholangiocarcinoma. HCC originates from malignant hepatocytes and is the predominant subtype of liver cancer (3). Owing to the absence of overt early symptoms causing diagnostic delays, a large proportion of patients with HCC present with advanced-stage disease at diagnosis (4).

Epigenetic alterations have a far higher risk of cancer compared with genetic mutations (5,6). Epigenetic regulators serve a key role in gene regulation, and the aberrant expression of epigenetic regulators, including DNA methylation machinery, polycomb proteins, chromatin remodellers and CCCTC-binding factor (CTCF), alter gene expression, cell differentiation and proliferation, thereby facilitating cancer development and progression (7). Identifying the key epigenetic regulators in cancer may enhance diagnostic sensitivity and specificity. Epigenetic therapy is a novel strategy for tumor treatment. Various epigenetic-targeting agents have entered clinical use for diverse malignancies, underscoring their clinical utility and therapeutic potential in cancer treatment (8).

Pioneer transcription factors drive closed chromatin remodeling either independently or through the recruitment of chromatin-modifying enzymes (9). Their involvement in cancer development has gained increasing attention (10-12). p63 has since been identified as a pioneer transcription factor (13). Previous studies have primarily focused on the role of p63 in epithelial cells and its upregulation in squamous cell carcinomas (14-16). Despite extensive research regarding types of cancer such as esophageal squamous cell carcinoma (17) and breast cancer (18), the function of p63 in liver cancer remains incompletely understood. Recent work has highlighted the oncogenic role of p63 in intrahepatic cholangiocarcinoma (19) and to further clarify its function in liver cancer, this investigation has been extended to HCC.

As a transcription factor not typically expressed in normal hepatocytes (20), the role of p63 in HCC remains unclear, with inconsistent reports regarding its expression in tumor tissues. For example, González *et al* (21) reported p63 expression in HCC cells, whereas Ramalho *et al* (22) reported none detected. The present study aimed to elucidate the oncogenic role and molecular functions of ΔNp63α in HCC using The Cancer Genome Atlas (TCGA)-based clinical analysis, functional assays, transcriptome profiling, ChIP-seq and ATAC-seq to characterize ΔNp63α-regulated gene programs and its associated chromatin regulatory mechanisms. ΔNp63α is the predominant variant in types of epithelial cancer and has been widely implicated in oncogenic processes (23,24). Therefore, the ΔNp63α isoform was selected for downstream functional characterization.

Materials and methods

Human data retrieval and analysis. p63 expression and its association with clinicopathological characteristics in HCC were analyzed using the University of Alabama at Birmingham Cancer data analysis Portal (UALCAN) (25,26) and Gene Expression Profiling Interactive Analysis 2 (GEPIA2) (27). Public multi-omics data, including mRNA and long non-coding (lncRNA) expression data and clinical data pertaining to patients diagnosed with HCC, were sourced from The Cancer Genome Atlas (TCGA) research network (https://portal.gdc.cancer.gov/) (28). These data were subsequently utilized to classify patients with HCC into Cluster 1, 2 and 3 using Multi-Omics Integration and Visualization in Cancer Subtyping (MOVICS) analysis (29). Within each of these HCC subtypes, the patients were further stratified into p63-high and p63-low expression groups, based on the median p63 expression level. The Kaplan-Meier method was used to compare survival outcomes between the groups. $P<0.05$ was considered to indicate a statistically significant difference. To externally validate the context-dependent prognostic relevance of p63, two independent HCC cohorts, GSE14520 (ncbi.nlm.nih.gov/geo/query/acc.cgi?acc=GSE14520) and GSE76427 (ncbi.nlm.nih.gov/geo/query/acc.cgi?acc=GSE76427), were obtained from the Gene Expression Omnibus (GEO) (30,31). The patients were stratified into p63-high and p63-low groups according to the expression level of the corresponding probe. Kaplan-Meier analysis was performed to assess the association between p63 expression and overall survival in the overall cohort and in clinically defined subgroups (stage I, II and III). Differences in survival between groups were assessed and $P<0.05$ was considered to indicate a statistically significant difference.

Cell culture. HCC cell lines HuH7 (cat. no. SCSP-526), PLC/PRF/5 (SCSP-5095), SNU182 (SCSP-5047), HCCLM3 (SCSP-5093), Hep3B (SCSP-5045), SNU387 (SCSP-5046) and MHCC97H (SCSP-5092), as well as the liver cancer cell line SK-Hep-1 (SCSP-5281), were obtained from the Cell Bank of the Chinese Academy of Sciences. The immortalized normal liver cell line MIHA was purchased from Guangzhou Tuoshan Biotechnology Co., Ltd. The immortalized human keratinocyte cell line HaCaT was obtained from Shanghai Anwei Biotechnology Co., Ltd. Cells were cultured in RPMI 1640 medium (Gibco; Thermo Fisher Scientific, Inc.), supplemented with 10% FBS (Gibco; Thermo Fisher Scientific, Inc.) and 100 U/ml penicillin/streptomycin (Gibco; Thermo Fisher Scientific, Inc.), at 37˚C in an incubator with 5% CO_2 and 95% humidity. The culture medium was replaced every 2 days. *Mycoplasma* contamination was not detected during cell culture, as assessed using the MycoBlue Mycoplasma Detector (Vazyme Biotech Co., Ltd.).

Lentiviral-mediated ΔNp63α overexpression (OE) and p63 knockdown (KO) in HCC cells. Lenti-Pac™ 293Ta packaging cell line (GeneCopoeia, LT008) was used as the transient packaging cell line. Lentiviral particles were generated using the Lenti-Pac™ HIV Expression Packaging Kit (LT002, GeneCopoeia) according to the manufacturer's instructions. Transfer, packaging, and envelope plasmids were used at a mass ratio of 4:4:1, with a total plasmid amount of approximately 10 μg per 10 cm culture dish. Viral supernatants were collected 48-72 h after transfection and clarified by centrifugation at 4,000 x g for 25 min at 4˚C. For infection of target cells, the multiplicity of infection (MOI) was 10. SNU387 cells were infected with lentiviral particles carrying ΔNp63α expression constructs (pEZ-Lv201) to establish a p63-OE cell line (SNU387-OE). SNU387 cells infected with empty vectors were used as negative controls (SNU387-EV). Transduction was performed overnight (12 to 16 h) at 37˚C. Following infection, puromycin was used for selection of transduced cells at a working concentration of 2 μg/ml. After 3-7 days of puromycin selection, stable cell lines were established, and the puromycin concentration was decreased to 0.5 μg/ml for maintenance. Stable ΔNp63α OE was determined by reverse transcription-quantitative PCR (RT-qPCR) and western blotting analysis. Subsequent experiments, including chromatin immunoprecipitation sequencing (ChIP-seq), were performed ~14 days after lentiviral infection. To complement the gain-of-function experiments, SNU182 cells with relatively high endogenous p63 expression were transfected with lentiviral particles carrying a psi-LVRU6MP vector expressing short hairpin (sh)-TP63 (5'-GGATGAAGA TAGCATCAGAAA-3') to establish stable p63-KO cells (SNU182-sh). SNU182 cells transfected with a non-targeting scrambled shRNA sequence (5'-GCTTCGCGCCGTAGTCTT A-3') were used as negative controls. KO efficiency was determined by RT-qPCR and western blotting analysis. Subsequent functional assays were performed using these established stable cell models.

Western blotting. Cells (HuH7, PLC/PRF/5, SNU182, HCCLM3, Hep3B, SNU387 and MHCC97H, SK-Hep-1, MIHA, HaCaT) were lysed in RIPA buffer (Thermo Fisher Scientific, Inc.) supplemented with protease inhibitors (Thermo Fisher Scientific, Inc.). After centrifugation, the supernatants were isolated, and the protein concentration was quantified using a BCA Kit (Thermo Fisher Scientific, Inc.). The proteins were separated by 10% SDS-PAGE, transferred to PVDF membranes, and blocked with 5% BSA. Membranes were probed with primary antibodies: Anti-p63: ΔNp63 (E6Q3O) rabbit monoclonal antibody (cat. no. 67825; Cell Signaling Technology) and anti-actin (cat. no. KC-5A08; Aksomics Inc.) at 4˚C overnight, then with secondary antibody: goat anti-rabbit

IgG H&L (HRP) (cat. no. ab6721; Abcam; 1:10,000) at room temperature for 1 h. Immunoblots were visualized using an Omega LumC imaging system with Immobilon western chemiluminescent HRP substrate (MilliporeSigma; Merck KGaA).

Extraction of total RNA and quantitation by RT-qPCR. Total RNA was extracted from HCC cells using TRIzol® reagent (Invitrogen; Thermo Fisher Scientific, Inc.) and subsequently converted to cDNA using the HiScript 1st Strand cDNA Synthesis Kit (cat. no. R111-01; Vazyme Biotech Co., Ltd.). The reverse transcription reaction was performed at 37˚C for 2 min, 55˚C for 15 min and 85˚C for 5 min. Quantitative assessment of RNA expression was conducted through RT-qPCR using SYBR® Premix Ex Taq™ II (Takara Biotechnology Co., Ltd.) and the ABI 7300 Real-Time Fluorescence PCR Detection System (Applied Biosystems; Thermo Fisher Scientific). The RT-qPCR conditions were as follows: 95˚C for 30 sec, followed by 40 cycles of 95˚C for 5 sec and 60˚C for 30 sec. RNA expression was normalized to GAPDH levels and quantification was achieved using the $2^{-\Delta\Delta Cq}$ method (32). The following RT-qPCR primers were used: p63 forward, 5'-CCAGAAGAAAGGACAGCAGC-3' and reverse, 5'-CAGGTTCGTGTACTGTGGCT-3'; GADPH forward, 5'-ACAACTTTGGTATCGTGGAAGG-3' and reverse, 5'-GCCATCACGCCACAGTTTC-3'.

Cell proliferation assay with cell counting kit-8 (CCK-8). Cells (SNU387-OE, SNU387-EV; SNU182-sh, SNU182-scr) were seeded in a 96-well culture plate at a density of 1,000 cells/well, with six replicate wells for each condition. After 24, 48 and 72 h of incubation, the total number of cells in each well was counted using a CCK-8 kit (Beyotime Biotechnology) following the manufacturer's protocol. Absorbance values were recorded at 450 nm. Each experiment was repeated six times independently to ensure reproducibility.

Colony formation assay. Cells (SNU387-OE, SNU387-EV) were plated in six-well plates at a density of 1,000 cells/well in triplicate and the culture medium was replaced every 2 days. After a 14-day incubation period, during which macroscopic colonies became visible, the spent culture medium was discarded, and the cells were carefully washed with PBS. Subsequently, the cells were fixed with 4% paraformaldehyde for 15 min and stained with crystal violet for 20 min, both at room temperature. Colonies were defined as discrete, darkly stained regions with a diameter >1 mm, and were counted using ImageJ software 1.54p (National Institutes of Health).

Wound healing assay. Cells (SNU387-OE, SNU387-EV; SNU182-sh, SNU182-scr) were seeded into six-well plates at a density of 2,000,000 cells per well. A sterile pipette tip was used to create a linear scratch across the cell monolayer. The cells were cultured in RPMI 1640 medium containing 5% FBS at 37˚C. Images of the wounds were captured using a Zeiss inverted light microscope at 24 and 48 h post-scratching. Wound widths were measured using ImageJ software 1.54p (National Institutes of Health) to determine the percentage of wound closure over time. Each experiment was repeated three times independently to ensure the reliability of the results.

RNA sequencing (RNA-seq) and data analysis. RNA-seq analysis was performed as previously described (19). Purified mRNA from HCC cells was used for library construction. Libraries were prepared using the Fast RNA-seq Lib Prep Kit V2 (Catalog No. RK29991, Novogene). The libraries were initially quantified using a Qubit 2.0 Fluorometer and diluted to 1.5 ng/μl. Insert sizes were assessed using an Agilent 2100 Bioanalyzer, and the effective library concentrations were subsequently determined by RT-qPCR. Libraries with an effective concentration >2 nM were sequenced on an Illumina NovaSeq 6000 platform (Illumina, Inc.; 150 bp; paired-end) using the NovaSeq 6000 S4 Reagent kit v1.5 (cat. no. 20028312; Illumina, Inc.). Adapter sequences were removed from the FASTQ files using TrimGalore (github.com/FelixKrueger/TrimGalore) and cleaned reads were mapped to hg38 via Hisat2 (33). FeatureCounts (34) were used to quantify gene expression. Each RNA-seq experiment was repeated thrice to ensure reproducibility. The 'DESeq2' R package (35) was used for differential expression analysis, with P-values adjusted using the Benjamini-Hochberg method (for false discovery rate control). Significant differentially expressed genes (DEGs) were defined as adjusted $P<0.05$ and $\log_2$ (fold change) >1 (unless otherwise specified). Functional enrichment analyses, including Gene Ontology (GO) (https://geneontology.org/), Kyoto Encyclopedia of Genes and Genomes (KEGG) (https://www.kegg.jp/) and gene set enrichment analysis (GSEA) (https://www.gsea-msigdb.org/gsea/), were performed to annotate the biological functions of the DEGs.

ChIP-seq and data analysis. ChIP-seq was performed as previously reported (13). Chromatin from 4,000,000 cells was sheared using COVARIS. Sheared chromatin was assessed by 2% agarose gel electrophoresis to verify the expected fragment size distribution (200-500 bp), and processed using iDeal ChIP-seq kits (cat. no. C01010055; Diagenode SA) for p63 or CTCF, ChIP used 5 μl anti-p63 (cat. no. 67825; Cell Signaling Technology, Inc.) or ~1 μg anti-CTCF (cat. no. C15410210; Diagenode SA). The input DNA (total unimmunoprecipitated chromatin) was collected and sequenced as a control for non-specific background signals. Input samples were incorporated during peak calling to estimate the background signal and improve the specificity of binding site identification. Libraries were prepared using the TruePrep Index Kit V2 for Illumina (cat. no. TD202) and the TruePrep DNA Library Prep kit V2 for Illumina (TD503, both Vazyme Biotech). After 10-16 cycles of PCR amplification, the libraries were purified using the QIAquick Gel Extraction Kit (28704, Qiagen) and quantified using the Qubit 1× dsDNA HS Assay Kit (Q33230, Thermo Fisher Scientific). The final library concentration ranged from 5 to 15 ng/μl, with a total volume of approximately 22 μl. Libraries with an effective concentration >2 nM were sequenced on a NovaSeq system (Illumina, Inc.; 150 bp; paired-end). Raw sequencing reads were processed using Fastp (36) and aligned to the human reference genome (hg38) using Bowtie2 (37). Peaks were identified using Model-Based Analysis of ChIP-Seq 2 (MACS2) (38). Peaks from all replicates were integrated using the irreproducible discovery rate (IDR) (39) to generate IDR-ranked consensus peaks. To preserve a broad spectrum of candidate regulatory regions

for integrative analysis using RNA-seq, assay for transposase-accessible chromatin using sequencing (ATAC-seq) and motif analyses, the complete IDR-ranked peak set was used for downstream overlap and annotation analyses and the IDR ranking score was retained as a measure of reproducibility. ChIP-seq signal visualization was performed using deepTools (40). Motif occurrence analysis was performed using find individual motif occurrences (FIMO) from the MEME Suite (41) with a threshold of P=0.001. Additional visualizations were generated using R (version 4.4.3) (R Foundation for Statistical Computing) and IGV software (version 2.13.1) (UC San Diego and the Broad Institute of MIT and Harvard).

Assay for ATAC-seq and data analysis. ATAC-seq libraries were prepared using ~5x10^4 cells per sample. Cell pellets were washed once with ice-cold PBS and lysed in 50 μl ice-cold lysis buffer containing 10 mM Tris (pH 7.4), 10 mM sodium chloride, 3 mM magnesium chloride and 0.1% NP-40 prepared in diethyl pyrocarbonate-treated water. Following centrifugation at 500 x g for 10 min at 4˚C, the supernatant was removed and the nuclei-containing pellet was subjected to transposition. For the transposition reaction, the cell pellet was incubated with 25 μl 2X Tagment DNA buffer, 2.5 μl Tn5 transposase and 22.5 μl nuclease free H_2O at 37˚C for 30 min. Transposed DNA was purified using a MinElute PCR purification kit (Qiagen, Inc.) and eluted in 10 μl elution buffer (10 mM Tris buffer; pH 8.0). After PCR amplification of the transposed DNA, ATAC-seq libraries were purified using Ampure XP beads (cat. no. A63881; Beckman Coulter, Inc.) and subjected to paired-end sequencing (150-bp) using an Illumina NovaSeq platform (Illumina, Inc.). The raw sequencing reads were quality-filtered and adapter-trimmed using Fastp (36). The cleaned paired-end reads were aligned to the human reference genome (hg38) using Bowtie2 (37). Mitochondrial reads mapping to chrM and reads overlapping the Encyclopedia of DNA Elements (42) blacklist regions (ENCFF356LFX) were subsequently removed. Accessible chromatin regions were identified using MACS2 (38). Genome-wide ATAC-seq signal tracks were generated using deepTools and normalized to counts per million. Signal profiles around transcription start sites and selected genomic regions were generated using deepTools.

Statistical analysis. All data are presented as the mean ± standard deviation of ≥3 independent experiments. Statistical analyses were performed using GraphPad Prism 9.0 (Dotmatics), and R 4.4.3 (R Foundation for Statistical Computing) through RStudio (Posit Software, PBC). Correlations between variables were analyzed using Pearson correlation analysis. Differences between groups were assessed using Student's t-tests or two-way ANOVA (with Tukey's post hoc test). Survival analysis was performed by employing the Kaplan-Meier method, with group differences assessed by the log-rank test. P<0.05 was considered to indicate a statistically significantly difference.

Results

Association between p63 expression and survival outcomes in patients with HCC. To explore the role of p63 in HCC development and progression, the expression in patients with HCC was analyzed. UALCAN analysis revealed that the overall p63 expression was relatively low in HCC; however, p63 expression was significantly enhanced in tumor tissues (n=371) compared with that in normal tissues (n=50; Fig. S1A). No significant difference in survival rates was detected based on p63 levels in the overall HCC patient cohort (Fig. S1B).

GEPIA2 analysis provided a more detailed view of p63 expression in individual HCC (n=367) and normal (n=160) samples. The expression distribution showed notable tailing in the high-expression region (Fig. S2A), suggesting certain patients with HCC exhibited elevated p63 levels. Based on the HCC subtypes available in GEPIA2 (27), patients with high p63 expression in iCluster1 (n=57) displayed significantly lower survival rates compared with those exhibiting low p63 expression; this was not observed in iCluster2 or iCluster3 (Fig. S2B). The HCC subtypes were derived from a previous study that used unsupervised clustering to classify HCC into different subgroups based on multi-omics data, including DNA copy number, DNA methylation, mRNA expression, miRNA expression and reverse-phase protein array proteomics data (43), allowing a comprehensive classification of patients with HCC.

MOVICS analysis (29) was performed, which requires only two multi-omics datasets for tumor subclassification; the mRNA and lncRNA expression data from 303 patients with HCC in TCGA-liver hepatocellular carcinoma (LIHC) dataset was used (28). This allowed the retention of more patients with HCC in the analysis after classifying them into different subtypes, providing a more nuanced view of the association between p63 expression and HCC subtypes. After obtaining an optimal cluster number of three for the HCC patient data (Fig. 1A), this optimal number was validated by applying a number of clustering methods (Fig. 1B). All of these methods demonstrated distinct clustering patterns when the HCC patient group was subdivided into three subtypes (Fig. 1B). Using the iClusterBayes clustering method implemented in the MOVICS framework, three molecular clusters were identified among the 303 patients with HCC: Cluster 1, 2 and 3. The clinical characteristics of these patients and their distribution across the three clusters are summarized in Tables I and II, respectively. Cluster 1 exhibited a lower proportion of stage I tumors and relatively higher proportions of stage II-III tumors compared with Cluster 3, which contained a higher proportion of early-stage cases (Table II), suggesting distinct clinical stage distributions between these clusters.

To characterize transcriptional differences among the three clusters, the 100 expressed genes with the greatest variance in mean expression across clusters were examined. Despite intracluster heterogeneity, Cluster 1 displayed a distinct expression profile, including relatively lower expression of hepatocyte-associated metabolic and secretory genes, such as hydroxysteroid 17-β dehydrogenase 13, aldolase, fructose-bisphosphate B, albumin, apolipoprotein (APO) C3, transthyretin and APOA1 (Fig. S3A). Pairwise differential-expression analyses comparing Cluster 1 with Cluster 2 and Cluster 3 identified consistently altered Cluster 1-associated genes (Fig. S3B). GSEA further showed that Cluster 1 was positively enriched for 'ribosome biogenesis', 'rRNA metabolic process', 'tRNA metabolic process' and 'protein-RNA

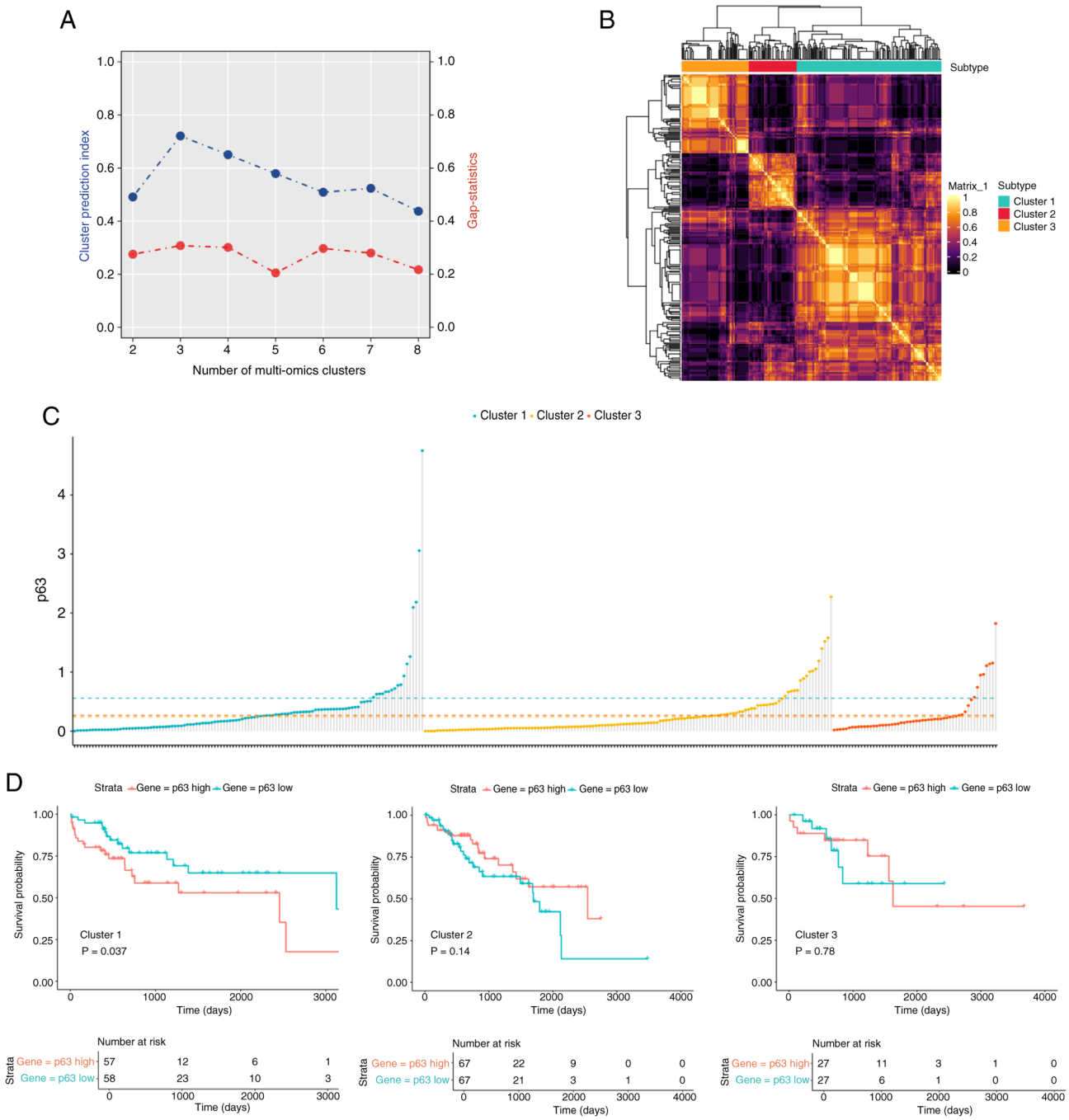


Figure 1. p63 expression in patients with HCC. (A) Multi-Omics Integration and Visualization in Cancer Subtyping framework was used to perform multi-omics data integration and classification of 303 patients with HCC. The optimal number of clusters was determined to be three. (B) Consensus clustering matrix representing the clustering results from 10 different multi-omics clustering algorithms: Cancer Integration through MultIkernel LeaRning, iClusterBayes, moCluster, Cluster-Of-Cluster-Assignments, ConsensusClustering, Integrative Clustering of Multiple Genomic Dataset, Landscape Reconstruction Algorithm, Neighborhood based Multi-Omics clustering, PINSPlus and Similarity network fusion. (C) Dot plots displaying p63 expression level in individuals from Cluster 1 to Cluster 3. The dashed lines indicate the average p63 expression level for each cluster. (D) Kaplan-Meier analysis was conducted to compare survival outcomes between patients with low and high p63 expression within the three HCC clusters. HCC, hepatocellular carcinoma.

complex assembly', whereas negatively enriched gene sets were associated with hepatocyte metabolic and secretory functions, including 'amino acid catabolic process', 'cholesterol metabolic process', 'fatty acid catabolic process' and 'plasma lipoprotein particle organization' (Fig. S3C-F). Collectively, these findings indicate that Cluster 1 is characterized by relative enrichment of RNA/protein biosynthetic programs, and attenuation of mature hepatocyte-associated metabolic and secretory programs.

The p63 expression levels were then assessed across the three clusters. As presented in Fig. 1C, Cluster 1 exhibited higher average p63 expression compared with Cluster 2 and Cluster 3. Kaplan-Meier survival analysis was performed to evaluate the association between p63 expression and overall survival. Patients within each cluster were divided into p63-high and p63-low groups according to the median p63 expression level. Within Cluster 1, the p63-high group showed significantly worse survival compared with the p63-low group,

Table I. Characteristics of 303 patients with hepatocellular carcinoma.

Variable	Classification
Age, years	
≥60	169 (55.78)
<60	132 (43.56)
NA	2 (0.66)
Sex (%)	
Female	100 (33.00)
Male	203 (67.00)
Stage (%)	
I	156 (51.49)
II	65 (21.45)
III	56 (18.48)
IV	3 (0.99)
NA	23 (7.59)
Survival outcome, (%)	
Deceased	92 (30.36)
Alive	211 (69.64)

whereas no significant association was observed in Clusters 2 or 3 (Fig. 1D). The association between other clinical variables, including sex age, weight and survival outcomes in Cluster 1 was further investigated, but none exhibited significant prognostic relevance (Fig. S4). Overall, Cluster 1 displayed distinct molecular characteristics derived from integrated multi-omics clustering, indicating relatively higher p63 expression and a distinct clinical stage distribution.

The prognostic relevance of p63 in two independent HCC cohorts (GSE14520 and GSE76427) was further validated. In the GSE14520 dataset, stage I patients with high p63 expression exhibited significantly worse overall survival. A similar association was observed in the GSE76427 cohort (Fig. S5). Consistent with the findings in Cluster 1, high p63 expression was associated with poorer overall survival in specific HCC subsets, but not in the overall cohort. Collectively, these results suggest that the prognostic effect of p63 is context-dependent and is not universally applicable across all patients with HCC.

Aberrant p63 expression affects the biological characteristics of HCC cells. First, the endogenous p63 protein expression in a panel of liver cancer-associated cell lines was examined. The tested cells included the HCC cell lines HUH7, PLC/PRF5, SNU182, HCCLM3, HEP3B, SNU387 and MHCC97H, as well as the liver cancer cell line SK-HEP-1. An immortalized human hepatocyte cell line was used as a negative control, whereas HaCaT cells, which exhibit high endogenous p63 expression (44), were used as a positive control. Western blotting analysis revealed that SNU182 cells exhibited relatively higher p63 protein expression compared with normal hepatocytes and other liver cancer-associated cells, whereas p63 protein levels were barely detectable in the majority of other cells (Fig. 2A). Subsequently, p63 mRNA expression was examined in immortalized human hepatocytes and liver cancer-associated cell lines, including HUH7, PLC/PRF5, SNU182, HCCLM3, HEP3B, SNU387 and SK-HEP-1, using qPCR assays. Consistent with the western blotting results, SNU182 exhibited the highest p63 transcript levels among the tested liver cancer-associated cell lines and displayed significantly higher expression compared with normal liver cells; the other cell lines exhibited relatively low p63 mRNA expression (Fig. 2B).

To explore the biological importance of p63 in HCC development and progression, SNU387 cells, which display low p63 expression were transfected, with the coding sequence of ΔNp63α to create a p63-overexpressing HCC cell line (SNU387-OE). SNU387 cells transfected with empty vectors served as the negative control (SNU387-EV). The mRNA and protein expression levels of p63 were analyzed in both SNU387-over and SNU387-vector cells (Fig. 2C and D), demonstrating successful OE in the SNU387-OE group.

Subsequently, CCK-8 assays were conducted to assess the effect of ΔNp63α OE on HCC cell proliferation. The results demonstrated enhanced proliferation of SNU387-OE cells compared with SNU387-EV cells (Fig. 2E). Furthermore, colony formation assays showed increased colony-forming capacity in SNU387-OE cells, consistent with the CCK-8 results (Fig. 2F). Wound healing assays further demonstrated significantly decreased wound areas in SNU387-OE compared with SNU387-EV cells, indicating enhanced migration ability (Fig. 2G), indicating that ΔNp63α OE promotes proliferative and migratory phenotypes in HCC cells. In addition, p63 KO experiments in SNU182 cells, an HCC cell line with relatively high endogenous p63 expression, were performed. p63 depletion reduced cell proliferation and migration capacities compared with control cells (Fig. S6), providing complementary evidence supporting the functional contribution of p63 to HCC-associated cellular phenotypes. Collectively, these findings suggest that ΔNp63α contributes to aggressive cellular behaviors in HCC and support a tumor-promoting role of p63 in HCC progression.

Transcriptome analysis of HCC cells after ΔNp63α OE. To investigate the effects of ΔNp63α on global gene expression in HCC cells, RNA-seq analysis was conducted on SNU387-OE and SNU387-EV cells. Each experiment was performed in triplicate. Hierarchical clustering analysis clearly separated the RNA-seq data into two distinct clusters: SNU387-OE and SNU387-EV (Fig. 3A). Correlation analysis demonstrated high reproducibility among the triplicate samples within each group (Fig. 3B).

A total of 4,978 significant DEGs were identified between the SNU387-OE and SNU387-EV samples, as presented in the volcano plot (Fig. 3C). The top 50 most variable genes across the samples are displayed in a heatmap (Fig. S7). Among the 21,532 transcripts quantified by RNA-seq, 23.12% (2,179 upregulated and 2,799 downregulated) were identified as significant DEGs, indicating that ΔNp63α serves a key role in regulating gene expression networks in HCC cells.

A number of functional enrichment analyses were performed to explore the biological functions of DEGs. GSEA in the Hallmark category revealed significantly enriched terms associated with tumorigenesis, such as 'HALLMARK_EPITHELIAL_MESENCHYMAL_TRANSITION', 'HALLMARK_KRAS_SIGNALING_UP' and

Table II. Basic information on different subtypes of patients with hepatocellular carcinoma.

Characteristic	Cluster 1 (n=115)	Cluster 2 (n=134)	Cluster 3 (n=54)
Age, years	60.90±12.49	60.5±13.42	60.07±13.25
Female, n (%)	39 (33.91)	46 (34.33)	15 (27.78)
Male, n (%)	76 (66.09)	88 (65.67)	39 (72.22)
Stage I, n (%)	50 (43.48)	71 (52.99)	35 (64.81)
Stage II, n (%)	33 (28.70)	26 (19.40)	6 (11.11)
Stage III, n (%)	24 (20.87)	23 (17.16)	9 (16.67)
Stage IV, n (%)	0 (0.00)	3 (2.24)	0 (0.00)
Mortality event, n (%)	37 (32.17)	42 (31.34)	13 (24.07)

Data are presented as mean ± SD for continuous variables and n (%) for categorical variables

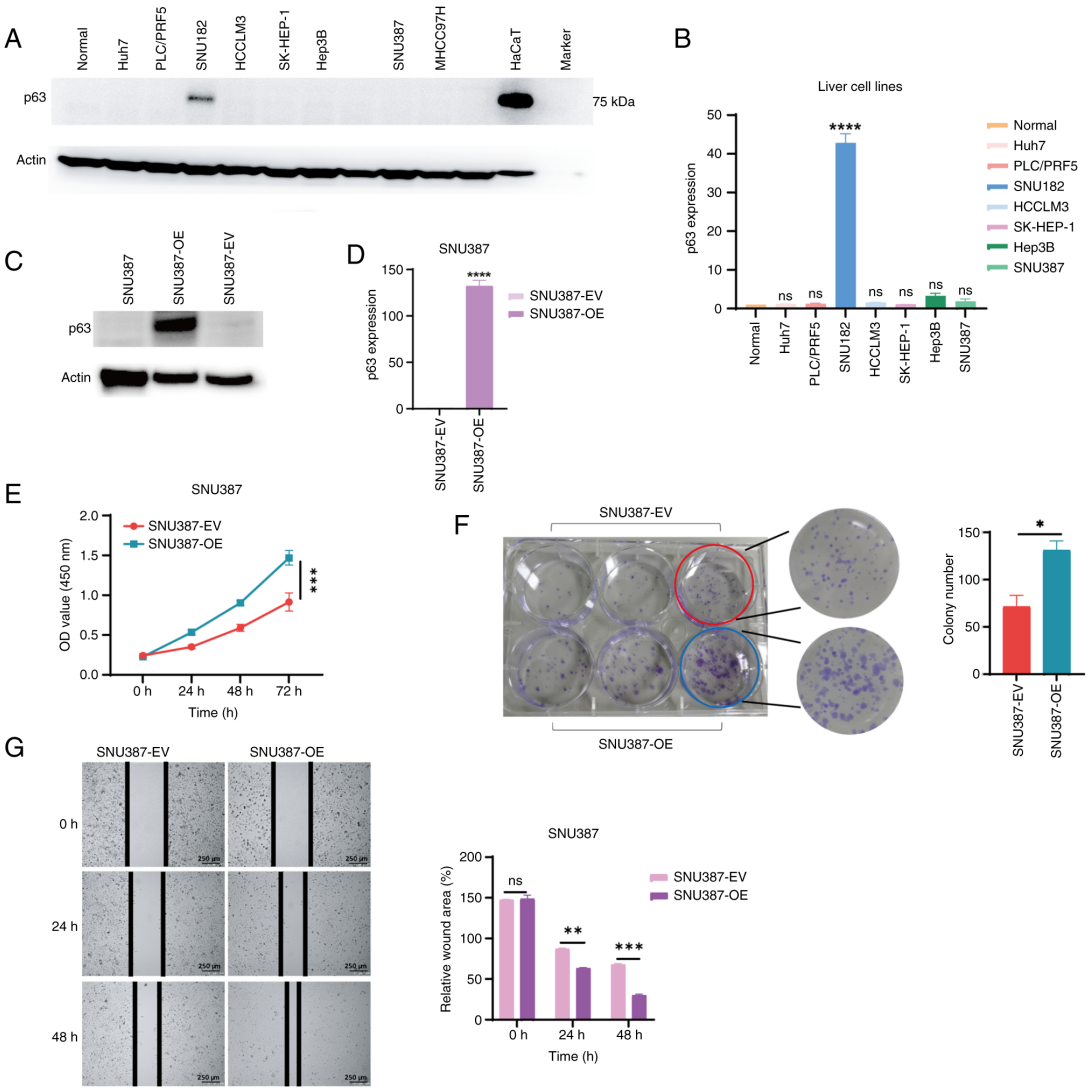


Figure 2. p63 expression and its impact on HCC cells. (A) Western blotting assay was conducted to examine p63 protein expression in human normal hepatocytes, liver cancer cells and different HCC cell lines. HaCaT cells served as the positive control, while normal hepatocytes were used as the negative control. (B) RT-qPCR was performed to quantify p63 mRNA levels in human normal hepatocytes, liver cancer cells and different HCC cell lines. Differences were considered statistically significant at P<0.05. (C) SNU387 cells were transfected with plasmids encoding ΔNp63α to establish the SNU387-OE cell line. Cells transfected with empty vectors were designated as SNU387-EV and western blot assay was conducted to determine p63 expression in transfected SNU387 cells. (D) RT-qPCR was performed to assess p63 mRNA level in SNU387 cells after transfection in both SNU387-OE and SNU387-EV cells. (E) Cell Counting Kit-8 assay indicating that OE of ΔNp63α significantly promoted the proliferation of SNU387 cells. (F) Colony formation assays were performed using SNU387-OE and SNU387-EV cells. The diameter of each well was ~35 mm. (G) Wound healing assay demonstrated that OE of ΔNp63α increased the migration ability of SNU387 cells (scale bar, 250 μm). The data presented are representative results from repeated experiments. P-values were calculated using the t-test, with asterisks indicating the level of statistical significance: *P<0.05, **P<0.01, ***P<0.001, ****P<0.0001 and ns, not significant. RT-qPCR, reverse transcription-quantitative PCR; OE, overexpression; EV, empty vector; HCC, hepatocellular carcinoma; OD, optical density.

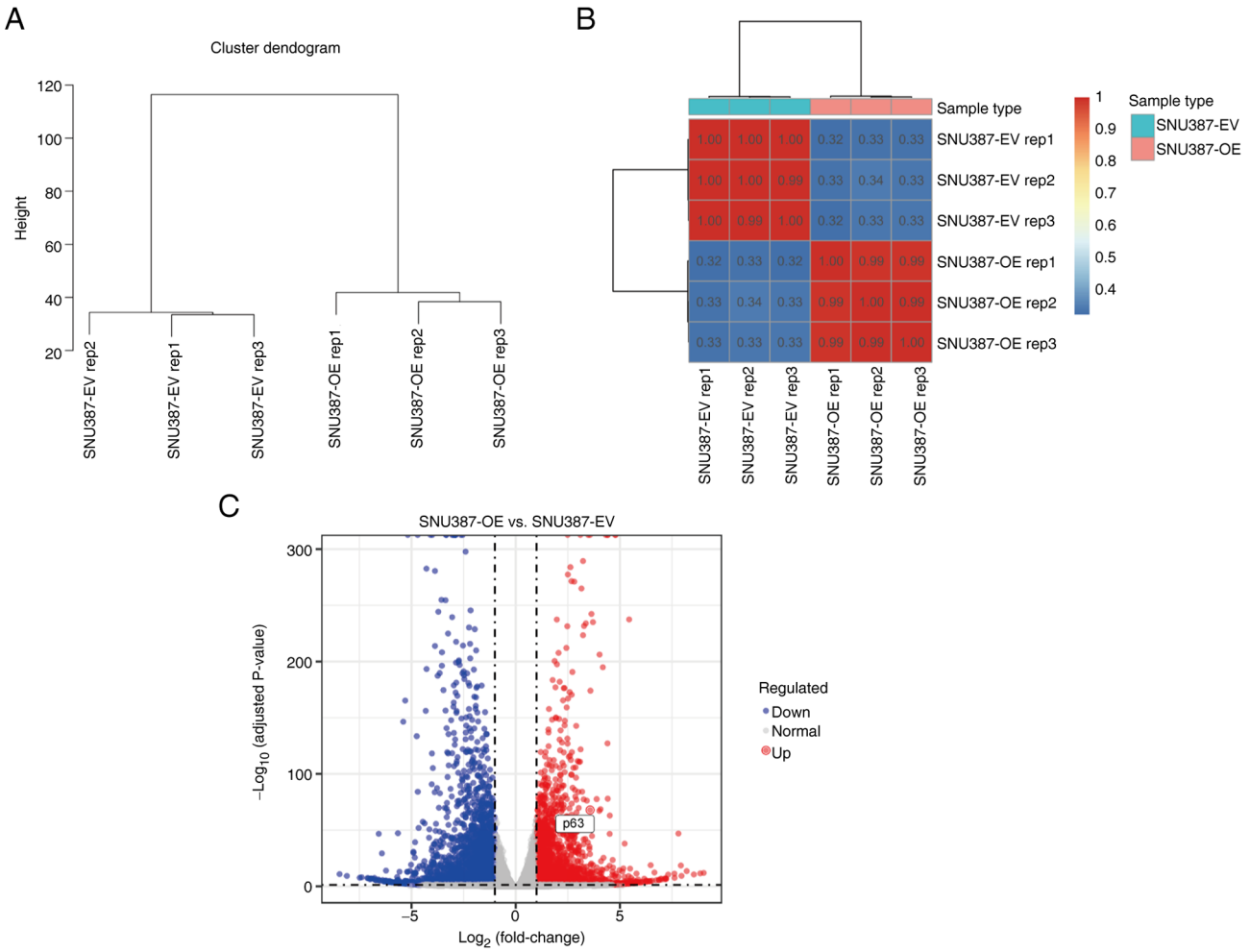


Figure 3. RNA-seq analysis in SNU387-OE and SNU387-EV cells. (A) Hierarchical clustering of RNA-seq data derived from triplicate experiments of SNU387-OE and SNU387-EV cells. (B) Correlation analysis demonstrated high reproducibility among replicate samples within each group. (C) Volcano plot showing differentially expressed genes between SNU387-OE and SNU387-EV cells [$\log_2$ (fold change) >1 and adjusted P<0.05]. The expression of p63 is indicated. RNA-seq, RNA-sequencing; up, upregulated; down, downregulated; OE, overexpression; EV, empty vector.

'HALLMARK_WNT_BETA_CATENIN_SIGNALING' (Fig. 4A). Conversely, protein secretion was suppressed, suggesting potential hepatocyte dysfunction and highlighting the complex role of ΔNp63α in HCC (Fig. 4A). In addition, analysis of the Reactome category revealed enrichment of pathways involved in cell proliferation and migration, including 'REACTOME_COLLAGEN_BIOSYNTHESIS_AND_MODIFYING_ENZYMES', 'REACTOME_NON_INTEGRIN_MEMBRANE_ECM_INTERACTIONS', 'REACTOME_INTEGRIN_CELL_SURFACE_INTERACTIONS' and 'REACTOME_EXTRACELLULAR MATRIX_ORGANIZATION' (Fig. 4B). A heatmap (Fig. 4C) was generated depicting the differential expression of genes involved in tumorigenesis and ECM-associated pathways across the samples. Almost all enriched genes involved in epithelial-mesenchymal transition, non-integrin-membrane ECM interactions, integrin cell surface interactions and ECM organization pathways were significantly upregulated (Fig. 4D), indicating the potential regulatory role of ΔNp63α in modulating these genes.

Subsequently, significantly upregulated genes upon ΔNp63α OE were identified and GO enrichment analysis was conducted to further investigate their functional roles in HCC. The results showed significant enrichment in the biological process category, with 'Wnt signaling pathway', 'cell-substrate adhesion' and 'extracellular matrix organization' ranking among the top ten enriched terms (Fig. 5A). Similarly, the top molecular function terms were 'extracellular matrix binding' and 'extracellular matrix structural constituent', whereas the cellular component category highlighted 'adherens junction' and 'collagen-containing extracellular matrix' (Fig. 5A). These findings indicated that ΔNp63α notably influences ECM components and associated functions in HCC cells.

KEGG analysis uncovered enrichment in four main categories: Organismal systems, human diseases, environmental information processing and cellular processes (Fig. 5B). Notably, significant enrichment was observed in numerous specific pathways, including the 'Wnt signaling pathway', 'ECM-receptor interaction', 'cell adhesion molecules' and 'regulation of actin cytoskeleton', consistent with the GO analysis findings (Fig. 5A). Collectively, these findings suggested that ΔNp63α may promote HCC development by activating genes involved in cell adhesion and ECM organization.

ChIP-seq analysis of p63 binding sites in HCC cells. To explore ΔNp63α binding *in vivo*, ChIP-seq experiments were performed using two biological replicates of SNU387-OE and SNU387-EV,

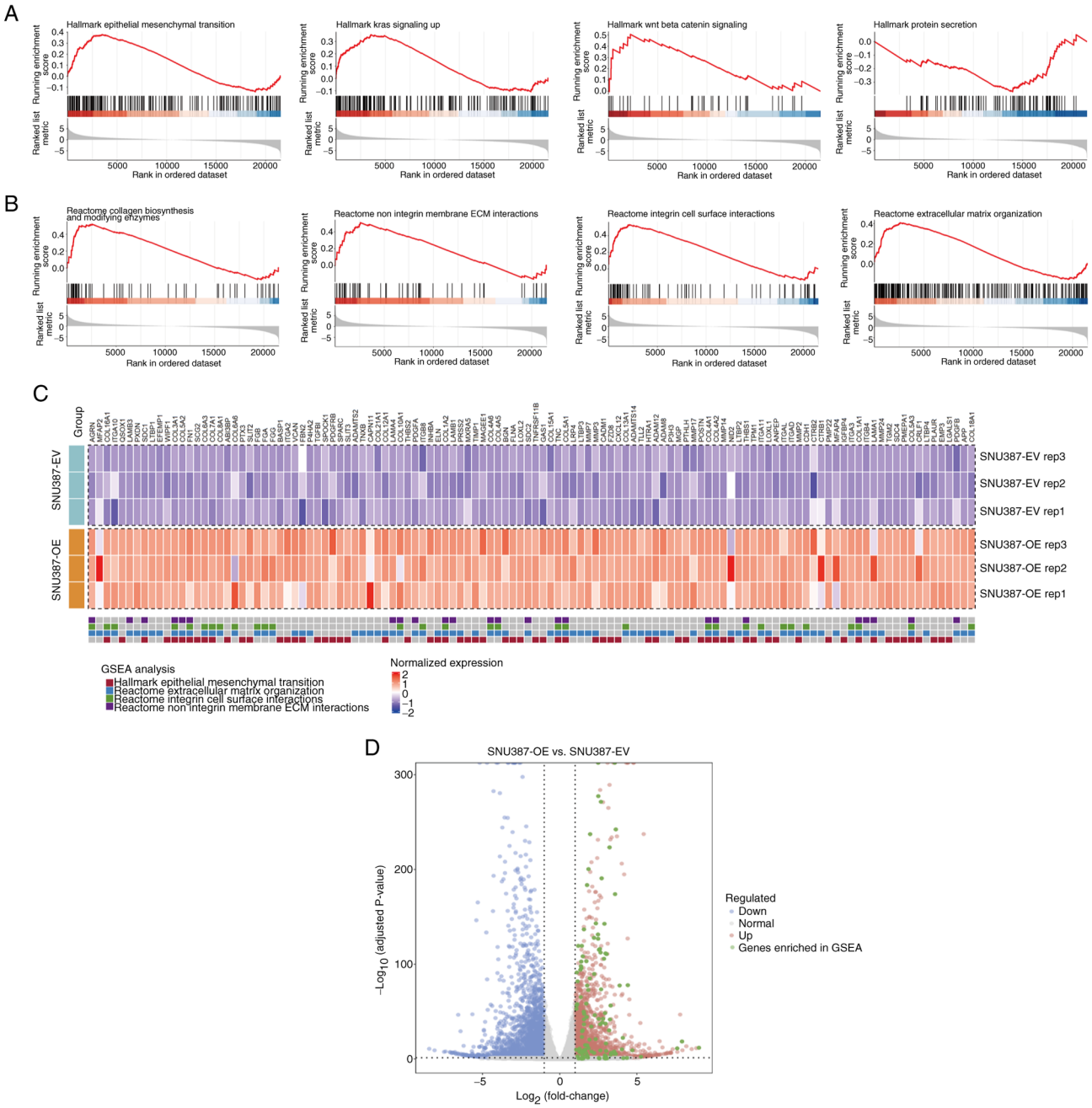


Figure 4. GSEA analysis of differentially expressed genes in SNU387-OE vs. SNU387-EV cells. (A) Significantly enriched pathways in the GSEA (A) Hallmark category. (B) Significantly enriched pathways in the GSEA Reactome category. (C) Heatmap of genes involved in representative GSEA-enriched pathways. (D) Volcano plot of all detected genes with $\log_2$ (fold change) as the x-axis and -$\log_{10}$ (adjusted P-value) as the y-axis. Upregulated DEGs and downregulated DEGs are shown in red and blue, respectively and genes associated with enriched GSEA pathways are highlighted in green. GSEA, gene set enrichment analysis; up, upregulated; down, downregulated; DEGs, differentially expressed genes.

respectively. Hereafter, p63 binding refers to ΔNp63α binding unless otherwise specified. In SNU387-OE cells, 23,818 sites were identified in replicate 1 and 14,010 sites in replicate 2 (Fig. 6). By contrast, very limited p63 binding was observed in SNU387-EV, with only 15 sites in replicate 1 and none in replicate 2. This was consistent with the barely detectable p63 protein expression in SNU387-EV. Metaplots and heatmaps further determined the absence and presence of p63 binding in the SNU387-EV and SNU387-OE cells, respectively (Fig. 6B).

Motif enrichment analysis showed that both SNU387-OE cell replicates were enriched in the p63 motif (Fig. 6C). CentriMo analysis demonstrated that the p63 motif was enriched at the center of the ChIP-seq peaks (Fig. 6D). IDR analysis was performed on the replicates to generate an IDR-ranked consensus peak list. After excluding the peaks present in SNU387-EV, 13,061 p63 binding sites specific to SNU387-OE cells were identified for subsequent analysis (Fig. 6E). To understand the characteristics of p63 binding, the binding signal around the transcription start site (TSS) was examined and slight enrichment as found (Fig. 6F). The distribution of p63 binding across the genome was then analyzed and found that <25% of binding sites were located within promoter-proximal regions (<3 kb from the TSS), whereas >50% were located in distal genomic regions (>10 kb

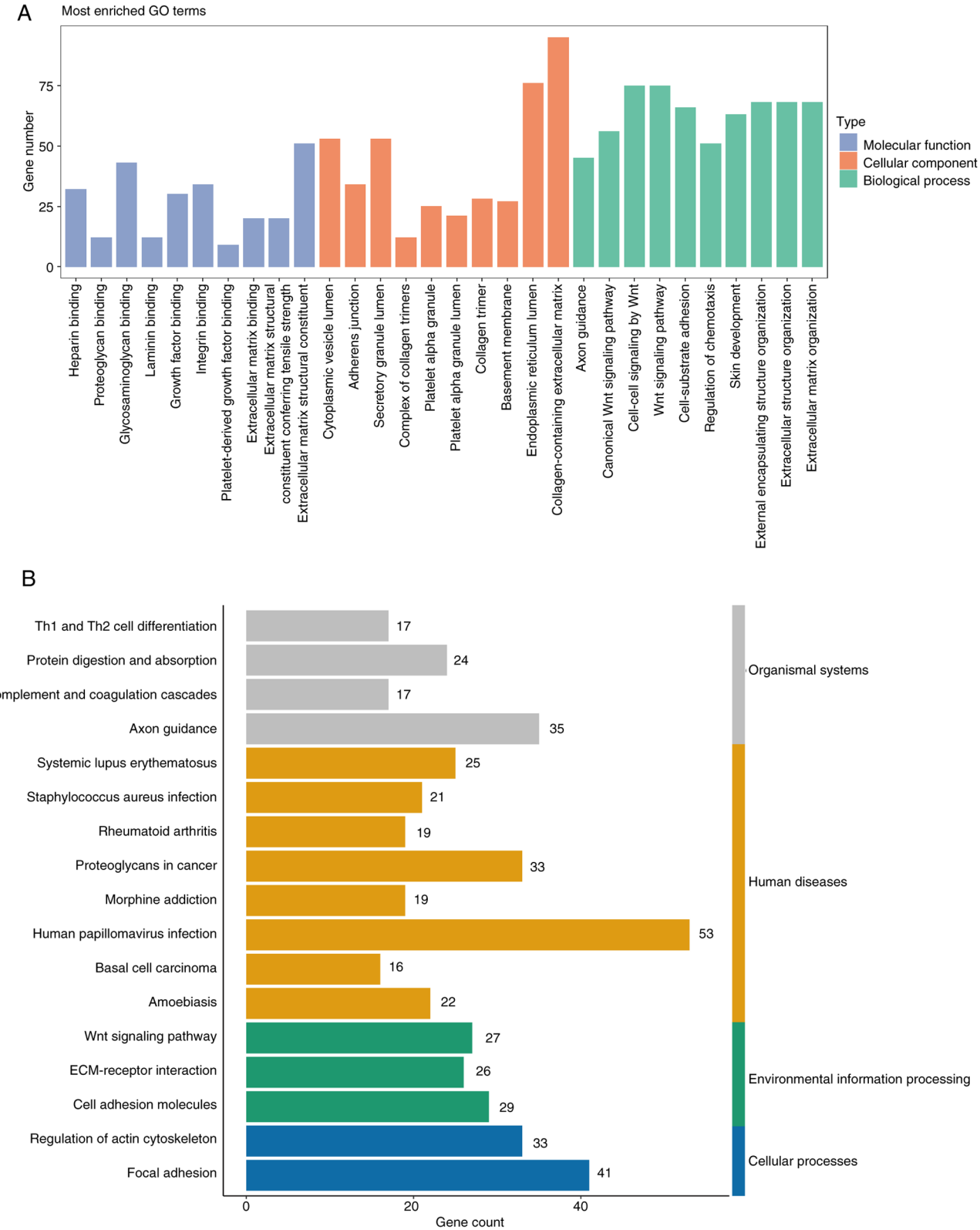


Figure 5. Functional enrichment analysis of significantly upregulated genes in SNU387-OE vs. SNU387-EV cells. (A) GO analysis identifying the enriched biological processes, molecular functions and cellular components among the significantly upregulated genes in SNU387-OE cells compared with SNU387-EV cells. (B) Kyoto Encyclopedia of Genes and Genomes analysis identifying enriched pathways and signaling networks among the significantly upregulated genes in SNU387-OE cells. OE, overexpression; EV, empty vector; GO, Gene Ontology; Th, T helper cells; ECM, extracellular matrix.

away from the TSS). This indicates that p63 binding predominantly occurs in distal genomic regions (Fig. 6G and H). The genomic distributions of p63 binding across the genome and the distributions of p63 binding sites relative to the TSS were compared between the two SNU387-OE replicates using χ^2 tests. No significant differences were detected between the replicates, supporting the consistency of the p63 ChIP-seq binding profiles (Tables SI-SIV).

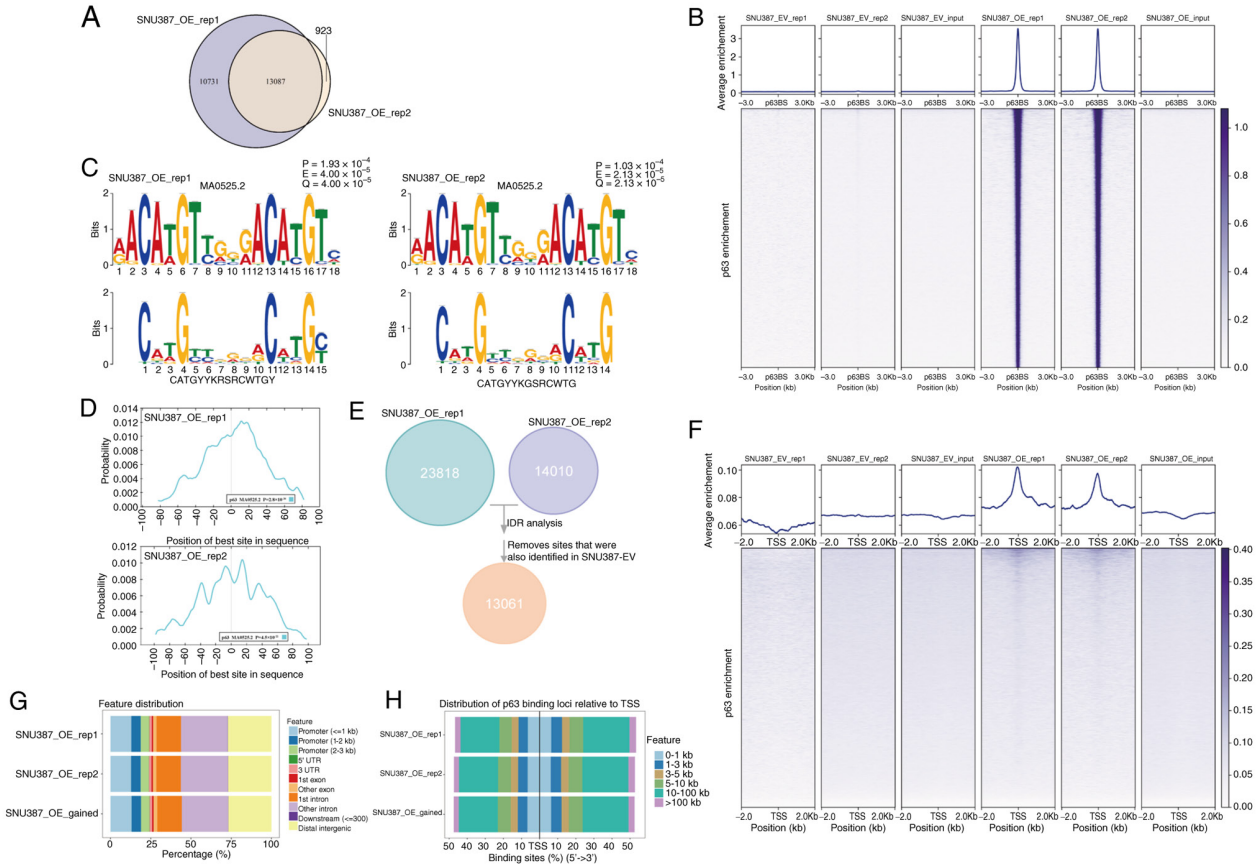


Figure 6. p63 ChIP-seq identifying genome-wide binding sites of ΔNp63α. (A) Venn diagram of the p63 ChIP-seq peaks identified in two replicates of SNU387-OE. (B) Heatmap of ChIP-seq signal across 3 kb upstream and 3 kb downstream of each p63 binding site, accompanied by the corresponding mean profiles in SNU387-OE and SNU387-EV cells. (C) Motif enrichment analysis revealing significant enrichment of the p63 motifs in both replicates of SNU387-OE. (D) CentriMo analysis demonstrating that p63 motifs were enriched at the center of the ChIP-seq peaks. (E) IDR analysis was performed to generate an IDR-ranked consensus peak list for SNU387-OE. Peaks unique to SNU387-OE were considered newly gained p63 binding sites. (F) Heatmap of p63 binding signals within 2 kb upstream and 2 kb downstream of each TSS, accompanied by the corresponding mean profiles in SNU387-OE and SNU387-EV cells. (G) Barplots illustrating the distribution of p63 binding sites across various genomic regulatory elements, comparing two replicates of SNU387-OE and gained p63 sites (SNU387-OE vs. SNU387-EV). No significant difference was observed between the two replicates (χ^2=2.4143; df=10; P=0.9921). (H) Barplots displaying the distance of p63 binding sites from the TSS in both replicates of SNU387-OE and gained p63 sites (SNU387-OE vs. SNU387-EV). No significant difference was observed between the two replicates (χ^2=4.7633; df=10; P=0.9064). OE, overexpression; EV, empty vector; ChIP-seq, chromatin immunoprecipitation sequencing; UTR, untranslated region; TSS, transcription start site; IDR, irreproducible discovery rate; df, degrees of freedom.

p63 binding at the promoter regions of significantly upregulated genes such as stratifin (SFN), serpin family B member 5 (SERPINB5), S100 calcium binding protein A2 (S100A2), FERM domain containing kindlin 1 (FERMT1) and keratin 5 was detected, suggesting transcriptional regulation by ΔNp63α. RNA-seq identified 10.12% (2,179 of 21,532) of genes as significantly upregulated (upDEGs), whereas promoter-proximal p63 binding (±2 kb from TSS) was observed in only 144 of these upDEGs. This suggests that ΔNp63α may also regulate a substantial proportion of target genes through distal regulatory elements rather than promoter-proximal binding alone. Previous studies have reported that p63 may influence chromatin architecture through interactions with architectural regulators such as CTCF to facilitate long-range chromatin interactions and enhancer-promoter communication (45,46). Therefore, whether CTCF binding was altered in response to ΔNp63α OE was investigated.

ΔNp63α influences CTCF binding in HCC cells. CTCF is a ubiquitously expressed protein that serves a role in mediating long-range promoter-enhancer interactions, influencing gene expression (47). Notably, CTCF binding close to promoters (promoter-proximal) can activate gene expression that is dependent on distal enhancers (48). Furthermore, previous research has demonstrated that p63 and CTCF cooperate to facilitate chromatin interactions between p63-bound enhancers and gene promoters (45). To investigate whether ΔNp63α upregulation influences CTCF occupancy, CTCF ChIP-seq was performed on both SNU387-OE and SNU387-EV cells. Compared with SNU387-EV, ΔNp63α OE resulted in increased CTCF binding in SNU387-OE, with elevated CTCF signals around both TSS and p63 binding sites (Fig. 7A and B). IDR analysis was performed on both replicates to generate an IDR-ranked consensus list of CTCF binding sites. After excluding peaks detected in SNU387-EV, 5,902 ΔNp63α-induced gained CTCF bindings were identified in SNU387-OE (Fig. 7C). Analysis of CTCF binding across the genome showed that these gained CTCF binding events were preferentially enriched in promoter-proximal regions compared with all CTCF binding sites (Fig. 7D), suggesting enhanced promoter-associated CTCF occupancy following ΔNp63α OE.

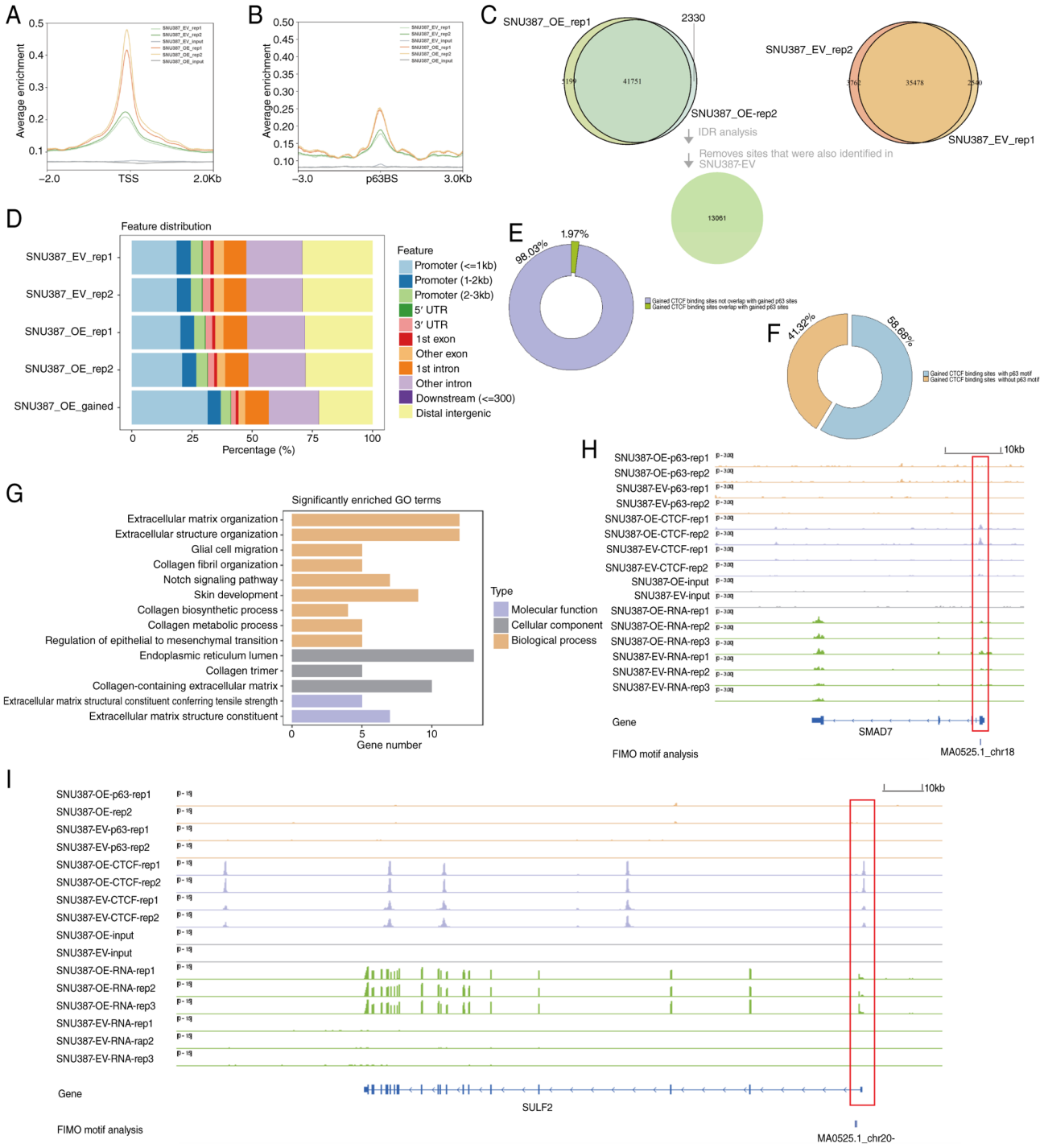


Figure 7. Effects of ΔNp63α OE on CTCF binding. (A) Profiles depicting the average CTCF binding signals spanning from 2 kb upstream to 2 kb downstream around the TSS in SNU387-OE and SNU387-EV cells. (B) Profiles displaying the average CTCF binding signals spanning from 2 kb upstream to 2 kb downstream around p63 binding sites in SNU387-OE and SNU387-EV cells. (C) Venn diagram comparing CTCF ChIP-seq peaks identified in SNU387-OE and SNU387-EV. IDR analysis was used to generate an IDR-ranked consensus peak list for SNU387-OE. Peaks unique to SNU387-OE were identified as ΔNp63α induced (newly gained) CTCF binding sites. (D) Barplots illustrate the distribution of CTCF binding sites across various regulatory elements in the genome, comparing SNU387-OE duplicates, SNU387-EV duplicates and gained CTCF sites (SNU387-OE vs. SNU387-EV). (E) Pie chart displaying the proportion of CTCF binding sites overlapping with p63 binding sites. (F) Pie chart displaying the proportion of CTCF binding sites containing p63 motifs. (G) GO analysis of gene promoters associated with CTCF binding sites containing the p63 motif. (H) IGV visualization of ChIP-seq and RNA-seq signals around the SMAD7 gene. (I) IGV visualization of ChIP-seq and RNA-seq signals around the SULF2 gene. Input sample signal tracks were also visualized in IGV. OE, overexpression; EV, empty vector; ChIP-seq, chromatin immunoprecipitation sequencing; RNA-seq, RNA-sequencing; CTCF, CCCTC-binding factor; TSS, transcription start site. FIMO, find individual motif occurrences; IDR, irreproducible discovery rate; SULF2, sulfatase 2.

Subsequently, the association between ΔNp63α and these newly acquired CTCF binding sites was investigated. Although only a limited number of newly gained p63 and CTCF peaks directly overlapped (Fig. 7E), motif analysis using FIMO identified p63 motifs (P<0.001) in 3,463 of the 5,902 gained CTCF binding sites (Fig. 7F). Furthermore,

among promoter-associated CTCF-gained sites associated with upregulated genes, 150 of 206 (72.8%) contained p63 motifs, representing a significant enrichment compared with the complete set of CTCF-gained sites (Fisher's exact test; odds ratio=1.89). These findings indicate that promoter-associated CTCF recruitment preferentially occurs in regulatory regions that harbor p63 recognition sequences.

The promoters (±2 kb from TSS) within these p63 motif-containing CTCF gained sites and identified associated genes were examined. Representative genes, including sulfatase 2, collagen type VIII α1 chain, collagen type XIII α1 chain, NOTCH1 and SMAD7, were significantly upregulated in the RNA-seq dataset and were enriched in biological processes associated with 'regulation of epithelial-to-mesenchymal transition', 'Notch signaling pathway' and 'extracellular matrix organization' (Fig. 7G). ChIP-seq signals were observed around a number of the aforementioned genes (Fig. 7H and I).

In addition, to determine whether ΔNp63α OE was associated with alterations in chromatin accessibility, ATAC-seq of SNU387-OE and SNU387-EV cells was performed. Genome-wide ATAC-seq profiling revealed a modest increase in chromatin accessibility around the TSS following ΔNp63α OE (Fig. S8A). Increased ATAC-seq signals were observed across the promoter regions of upregulated genes that overlapped with p63-gained or CTCF-gained binding sites, suggesting that ΔNp63α OE is associated with increased promoter accessibility at these regulatory regions (Fig. S8B-C).

Collectively, these findings support an association between ΔNp63α OE, increased promoter chromatin accessibility, preferential CTCF recruitment to p63 motif-containing regulatory regions, and the activation of downstream transcriptional programs.

Discussion

Liver cancer is a global health burden with high incidence and mortality rates, particularly in Asia (1). HCC, the predominant histological subtype, arises from hepatocytes and is characterized by marked molecular and clinical heterogeneity. This heterogeneity is driven by diverse genetic and epigenetic alterations, as well as dysregulated signaling pathways that contribute to tumor progression and therapeutic resistance (49). Despite advances in molecular profiling, reliable biomarkers, key regulatory drivers of HCC and clinical outcome prediction remain unclear.

p63, especially the ΔNp63 isoform, exhibits robust expression in epithelial cells, epithelial-rich tissues and types of epithelial cancer (50), acting as a lineage-specific master transcription factor involved in cell fate decisions, lineage commitment and epithelial stemness regulation (51). p63 is absent in normal liver tissues (52); however, its expression in HCC remains debatable (21,22). The biological role of p63 in HCC is incompletely understood, partly owing to the molecular heterogeneity of HCC, including variations in genomic, proteomic and metabolic profiles that influence clinical outcomes (53).

Molecular subclassification improves disease stratification and supports personalized therapy (54). In the present study, p63 upregulation was observed in TCGA-LIHC tumors and subtype-specific expression patterns were identified using integrative multi-omics clustering analysis. Three molecular subtypes were defined (Cluster 1-3). Cluster 1, characterized by relatively higher p63 expression and enrichment of intermediate-stage tumors, exhibited a significant association between p63 expression and survival, with worse outcomes observed in patients with high p63 expression. No such association was observed in Clusters 2 and 3. Consistent with this finding, external validation (GSE14520 and GSE76427) showed that the prognostic effect of p63 was restricted to the early-stage HCC subset (stage I).

These results suggest that p63 functions in a context-dependent manner in HCC rather than acting as a universal biomarker and that its prognostic relevance is influenced by both molecular subtype and clinical stage. Differences between the multi-center TCGA cohort and the external datasets likely reflect variations in cohort composition and clinical heterogeneity, including stage distribution and molecular background. Collectively, the present findings suggest that the biological and prognostic importance of p63 is context dependent, reflecting its role in regulating subtype-associated transcriptional programs rather than serving as a universal prognostic marker for HCC.

Notably, p63 expression in TCGA and the GEO datasets reflected bulk transcript abundance and did not distinguish between individual isoforms. ΔNp63α is the predominant and most well-characterized isoform in epithelial cancer (50,55). HCC originates from hepatocytes and retains epithelial features during tumor progression (56-58). Based on this biological context, ΔNp63α was selected as the representative isoform for the functional studies. Accordingly, the present functional analyses should be interpreted as isoform-specific mechanistic investigations rather than generalizations of total p63 activity. Other p63 isoforms may also contribute to tumor biology; however, their individual contributions cannot be reliably distinguished in the present bulk transcriptomic datasets due to sufficient isoform-specific resolution.

SNU387 cells with ΔNp63α OE vectors (SNU387-OE) or empty vectors (SNU387-EV), were constructed to investigate the functional role of ΔNp63α in HCC. ΔNp63α OE significantly enhanced cell proliferation and migration, indicating its functional contribution to HCC aggressiveness. RNA-seq analysis revealed that >20% of genes were differentially expressed, indicating a broad transcriptional impact of ΔNp63α. Functional enrichment analysis showed significant enrichment of genes involved in tumor-associated pathways, including 'regulation of epithelial-to-mesenchymal transition', 'Wnt signaling pathway' and 'Notch signaling pathway', consistent with previous studies implicating p63 in the regulation of these pathways (50,59). In addition, genes associated with 'regulation of actin cytoskeleton', 'cell adhesion molecules' and 'extracellular matrix organization' were significantly enriched, suggesting a role for ΔNp63α in regulating cell processes associated with proliferation and migration (60).

ChIP-seq analysis identified genome-wide ΔNp63α binding sites in SNU387 cells. Analysis of the p63-bound regions in SNU387-OE cells exhibited promoter-associated p63 binding at genes involved in epithelial migration (S100A2, EPH receptor B4, FERMT1 and KN motif and ankyrin repeat domains 1) (61-64) and proliferation (SFN, BAX, SERPINB5

and GLI family zinc finger 1) (65-68), suggesting these genes may represent direct transcriptional targets of ΔNp63α. Notably, only ~25% of binding sites were located at promoters, while >50% were in distal intergenic regions (>10 kb from TSS). This distribution is consistent with the established role of p63 in regulating both promoter activity and distal cis-regulatory elements.

CTCF was included as a hypothesis-driven candidate regulator in the present study, given its established role in 3D genome organization and prior reports suggesting cooperation with p63 in regulating tissue-specific enhancer-promoter interactions (45,46). As a core architectural protein, CTCF is mainly enriched at topologically associated domain boundaries rather than at classical enhancer-promoter elements (69), although context-dependent promoter-proximal binding linked to distal regulatory activity has also been reported (48). Previous studies have suggested that p63 cooperates with chromatin architectural regulators, including CTCF, to organize tissue-specific chromatin interactions and epithelial transcriptional programs (45,46).

In the present study, ΔNp63α OE was associated with increased promoter-proximal CTCF occupancy, whereas direct overlap between newly gained p63 and CTCF binding sites remained limited. This observation suggests that ΔNp63α and CTCF may regulate overlapping genomic regions through a dynamic functional association rather than persistent co-binding. Importantly, promoter-associated CTCF-gained sites were significantly enriched for p63 motifs compared with the complete set of CTCF-gained sites, indicating that the newly acquired promoter-associated CTCF preferentially occurred within p63-responsive regulatory sequences. Furthermore, ATAC-seq analysis demonstrated increased chromatin accessibility around the TSS and across the promoters of the activated genes following ΔNp63α OE. Together with p63 motif enrichment at promoter-associated CTCF gained sites, these findings support a model in which ΔNp63α may contribute to the establishment of a chromatin environment that is permissive for CTCF occupancy. Notably, genes associated with these promoter-associated CTCF binding events were transcriptionally upregulated upon ΔNp63α OE and were enriched in tumor-associated pathways, suggesting an association between promoter-associated CTCF occupancy and ΔNp63α-mediated transcriptional activation.

Collectively, these observations, together with emerging evidence associating p63-mediated chromatin looping and CTCF-associated epigenetic regulation in cancer (46,70,71), suggest that ΔNp63α OE is associated with increased promoter chromatin accessibility and promoter-proximal CTCF occupancy in p63 motif-enriched regulatory regions, thereby reshaping the transcriptional landscape of HCC. Despite integrative multi-omics analyses supporting an association between ΔNp63α activity and promoter-associated CTCF occupancy, these data do not establish a direct causal mechanism for CTCF recruitment. Future studies involving perturbation of p63 or CTCF, as well as chromatin conformation analyses, are required to define the mechanistic association between ΔNp63α-mediated chromatin remodeling and CTCF-associated regulation.

In summary, the present study identified ΔNp63α as a key regulator of tumor-associated transcriptional programs in HCC. By integrating RNA-seq, ChIP-seq and ATAC-seq analyses, the present study provides evidence that ΔNp63α OE is associated with increased promoter chromatin accessibility, enhanced promoter-proximal CTCF occupancy and activation of tumor-associated transcriptional programs. These findings provide new insight into how ΔNp63α may reshape the regulatory landscape of HCC and establish a foundation for future mechanistic studies.

Acknowledgements

Not applicable.

Funding

The present study received funding from the National Natural Science Foundation of China (grant no. 32100447), the Guangdong Basic and Applied Basic Research Foundation (grant no. 2022A1515011932) and the Zhuhai People's Hospital Xiangshan Scholars Research Foundation (grant no. 2020XSYC-03).

Availability of data and materials

The data generated in the present study may be found in the NCBI Sequence Read Archive under BioProject accession numbers PRJNA1197994 (persistent, https://www.ncbi.nlm.nih.gov/bioproject/PRJNA1197994) and PRJNA1497660 (persistent, https://www.ncbi.nlm.nih.gov/bioproject/PRJNA1497660).

Authors' contributions

XY conceived and designed the study. XL and AP performed the cell culture, RT-qPCR, next-generation sequencing and western blotting experiments. XL and AP confirm the authenticity of all the raw data. XY performed the bioinformatic analyses of next-generation sequencing data. XY, XL, MZ and AP interpreted the results. XY drafted the manuscript. All authors read and approved the final version of the manuscript.

Ethics approval and consent to participate

Not applicable.

Patient consent for publication

Not applicable.

Competing interests

The authors declare that they have no competing interests.

Use of artificial intelligence tools

During the preparation of this work, artificial intelligence tools were used to improve the readability and language of the manuscript, and subsequently the authors revised and edited the content produced by the artificial intelligence tools as necessary, taking full responsibility for the ultimate content of the present manuscript.

References

1. Singal AG, Kanwal F and Llovet JM: Global trends in hepatocellular carcinoma epidemiology: Implications for screening, prevention and therapy. Nat Rev Clin Oncol 20 864-884, 2023.
2. Bray F, Laversanne M, Sung H, Ferlay J, Siegel RL, Soerjomataram I and Jemal A: Global cancer statistics 2022: GLOBOCAN estimates of incidence and mortality worldwide for 36 cancers in 185 countries. CA Cancer J Clin 74: 229-263, 2024.
3. Brunt E, Aishima S, Clavien PA, Fowler K, Goodman Z, Gores G, Gouw A, Kagen A, Klimstra D, Komuta M, *et al*: cHCC-CCA: Consensus terminology for primary liver carcinomas with both hepatocytic and cholangiocytic differentation. Hepatology 68: 113-126, 2018.
4. Patel N, Yopp AC and Singal AG: Diagnostic delays are common among patients with hepatocellular carcinoma. J Natl Compr Canc Netw 13: 543-549, 2015.
5. Sadida HQ, Abdulla A, Marzooqi SA, Hashem S, Macha MA, Akil ASA and Bhat AA: Epigenetic modifications: Key players in cancer heterogeneity and drug resistance. Transl Oncol 39: 101821, 2024.
6. Takeshima H and Ushijima T: Accumulation of genetic and epigenetic alterations in normal cells and cancer risk. NPJ Precis Oncol 3: 7, 2019.
7. Cavalli G and Heard E: Advances in epigenetics link genetics to the environment and disease. Nature 571: 489-499, 2019.
8. Cheng Y, He C, Wang M, Ma X, Mo F, Yang S, Han J and Wei X: Targeting epigenetic regulators for cancer therapy: Mechanisms and advances in clinical trials. Signal Transduct Target Ther 4: 62, 2019.
9. Barral A and Zaret KS: Pioneer factors: Roles and their regulation in development. Trends Genet 40: 134-148, 2024.
10. Sunkel BD and Stanton BZ: Pioneer factors in development and cancer. iScience 24: 103132, 2021.
11. Hankey W, Chen Z and Wang Q: Shaping chromatin states in prostate cancer by pioneer transcription factors. Cancer Res 80: 2427-2436, 2020.
12. Pavithran H and Kumavath R: Emerging role of pioneer transcription factors in targeted ERα positive breast cancer. Explor Target Antitumor Ther 2: 26-35, 2021.
13. Yu X, Singh PK, Tabrejee S, Sinha S and Buck MJ: ΔNp63 is a pioneer factor that binds inaccessible chromatin and elicits chromatin remodeling. Epigenetics Chromatin 14: 20, 2021.
14. Manzella L, Stella S, Pennisi MS, Tirrò E, Massimino M, Romano C, Puma A, Tavarelli M and Vigneri P: New insights in thyroid cancer and p53 family proteins. Int J Mol Sci 18: 1325, 2017.
15. Candi E, Cipollone R, Rivetti di Val Cervo P, Gonfloni S, Melino G and Knight R: p63 in epithelial development. Cell Mol Life Sci 65: 3126-3133, 2008.
16. Zhang Y, Karagiannis D, Liu H, Lin M, Fang Y, Jiang M, Chen X, Suresh S, Huang H, She J, *et al*: Epigenetic regulation of p63 blocks squamous-to-neuroendocrine transdifferentiation in esophageal development and malignancy. Sci Adv 10: eadq0479, 2024.
17. Yu VZ, So SS, Lung BC, Hou GZ, Wong CW, Chow LK, Chung MK, Wong IY, Wong CL, Chan DK, *et al*: ΔNp63-restricted viral mimicry response impedes cancer cell viability and remodels tumor microenvironment in esophageal squamous cell carcinoma. Cancer Lett 595: 216999, 2024.
18. Alkhayyat R, Abbas A, Quinn CM and Rakha EA: Tumour 63 protein (p63) in breast pathology: Biology, immunohistochemistry, diagnostic applications, and pitfalls. Histopathology 84: 723-741, 2024.
19. Peng A, Lin X, Yang Q, Sun Y, Chen R, Liu B and Yu X: ΔNp63α facilitates proliferation and migration, and modulates the chromatin landscape in intrahepatic cholangiocarcinoma cells. Cell Death Dis 14: 777, 2023.
20. Uhlen M, Zhang C, Lee S, Sjöstedt E, Fagerberg L, Bidkhori G, Benfeitas R, Arif M, Liu Z, Edfors F, *et al*: A pathology atlas of the human cancer transcriptome. Science 357: eaan2507, 2017.
21. González R, De la Rosa ÁJ, Rufini A, Rodríguez-Hernández MA, Navarro-Villarán E, Marchal T, Pereira S, De la Mata M, Müller-Schilling M, Pascasio-Acevedo JM, *et al*: Role of p63 and p73 isoforms on the cell death in patients with hepatocellular carcinoma submitted to orthotopic liver transplantation. PLoS One 12: e0174326, 2017.
22. Ramalho FS, Ramalho LN, Della Porta L and Zucoloto S: Comparative immunohistochemical expression of p63 in human cholangiocarcinoma and hepatocellular carcinoma. J Gastroenterol Hepatol 21: 1276-1280, 2006.
23. Ram Kumar RM, Betz MM, Robl B, Born W and Fuchs B: ΔNp63α enhances the oncogenic phenotype of osteosarcoma cells by inducing the expression of GLI2. BMC Cancer 14: 559, 2014.
24. Sethi I, Romano RA, Gluck C, Smalley K, Vojtesek B, Buck MJ and Sinha S: A global analysis of the complex landscape of isoforms and regulatory networks of p63 in human cells and tissues. BMC Genomics 16: 584, 2015.
25. Chandrashekar DS, Bashel B, Balasubramanya SAH, Creighton CJ, Ponce-Rodriguez I, Chakravarthi BVSK and Varambally S: UALCAN: A portal for facilitating tumor subgroup gene expression and survival analyses. Neoplasia 19: 649-658, 2017.
26. Chandrashekar DS, Karthikeyan SK, Korla PK, Patel H, Shovon AR, Athar M, Netto GJ, Qin ZS, Kumar S, Manne U, *et al*: UALCAN: An update to the integrated cancer data analysis platform. Neoplasia 25: 18-27, 2022.
27. Tang Z, Kang B, Li C, Chen T and Zhang Z: GEPIA2: An enhanced web server for large-scale expression profiling and interactive analysis. Nucleic Acids Res 47: W556-W560, 2019.
28. Wang Z, Jensen MA and Zenklusen JC: A practical guide to the cancer genome atlas (TCGA). Methods Mol Biol 1418: 111-141, 2016.
29. Lu X, Meng J, Zhou Y, Jiang L and Yan F: MOVICS: An R package for multi-omics integration and visualization in cancer subtyping. Bioinformatics 36: 5539-5541, 2021.
30. Roessler S, Jia HL, Budhu A, Forgues M, Ye QH, Lee JS, Thorgeirsson SS, Sun Z, Tang ZY, Qin LX and Wang XW: A unique metastasis gene signature enables prediction of tumor relapse in early-stage hepatocellular carcinoma patients. Cancer Res 70: 10202-10212, 2010.
31. Grinchuk OV, Yenamandra SP, Iyer R, Singh M, Lee HK, Lim KH, Chow PK and Kuznetsov VA: Tumor-adjacent tissue co-expression profile analysis reveals pro-oncogenic ribosomal gene signature for prognosis of resectable hepatocellular carcinoma. Mol Oncol 12: 89-113, 2018.
32. Livak KJ and Schmittgen TD: Analysis of relative gene expression data using real-time quantitative PCR and the 2(-Delta Delta C(T)) method. Methods 25: 402-408, 2001.
33. Kim D, Paggi JM, Park C, Bennett C and Salzberg SL: Graph-based genome alignment and genotyping with HISAT2 and HISAT-genotype. Nat Biotechnol 37: 907-915, 2019.
34. Liao Y, Smyth GK and Shi W: featureCounts: An efficient general purpose program for assigning sequence reads to genomic features. Bioinformatics 30: 923-930, 2014.
35. Love MI, Huber W and Anders S: Moderated estimation of fold change and dispersion for RNA-seq data with DESeq2. Genome Biol 15: 550, 2014.
36. Chen S, Zhou Y, Chen Y and Gu J: fastp: An ultra-fast all-in-one FASTQ preprocessor. Bioinformatics 34: i884-i890, 2018.
37. Langmead B and Salzberg SL: Fast gapped-read alignment with Bowtie 2. Nat Methods 9: 357-359, 2012.
38. Zhang Y, Liu T, Meyer CA, Eeckhoute J, Johnson DS, Bernstein BE, Nusbaum C, Myers RM, Brown M, Li W and Liu XS: Model-based analysis of ChIP-Seq (MACS). Genome Biol 9: R137, 2008.
39. Landt SG, Marinov GK, Kundaje A, Kheradpour P, Pauli F, Batzoglou S, Bernstein BE, Bickel P, Brown JB, Cayting P, *et al*: ChIP-seq guidelines and practices of the ENCODE and modENCODE consortia. Genome Res 22: 1813-1831, 2012.
40. Ramírez F, Dündar F, Diehl S, Grüning BA and Manke T: deepTools: A flexible platform for exploring deep-sequencing data. Nucleic Acids Res 42: W187-W191, 2014.
41. Bailey TL, Johnson J, Grant CE and Noble WS: The MEME suite. Nucleic Acids Res 43: W39-W49, 2015.
42. ENCODE Project Consortium; Moore JE, Purcaro MJ, Pratt HE, Epstein CB, Shoresh N, Adrian J, Kawli T, Davis CA, Dobin A, *et al*: Expanded encyclopaedias of DNA elements in the human and mouse genomes. Nature 583: 699-710, 2020.
43. Cancer Genome Atlas Research Network. Electronic address: wheeler@bcm.edu; Cancer Genome Atlas Research Network Cancer Genome Atlas Research Network. Electronic address: wheeler@bcm.edu and Cancer Genome Atlas Research Network. Comprehensive and integrative genomic characterization of hepatocellular carcinoma. Cell1 69: 1327-1341.e23, 2017.

44. Testoni B and Mantovani R: Mechanisms of transcriptional repression of cell-cycle G2/M promoters by p63. Nucleic Acids Res 34: 928-938, 2006.
45. Qu J, Yi G and Zhou H: p63 cooperates with CTCF to modulate chromatin architecture in skin keratinocytes. Epigenetics Chromatin 12: 31, 2019.
46. Smirnov A, Lena AM, Tosetti G, Yang X, Cappello A, Helmer Citterich M, Melino G and Candi E: Epigenetic priming of an epithelial enhancer by p63 and CTCF controls expression of a skin-restricted gene XP33. Cell Death Discov 9: 446, 2023.
47. Ren G, Jin W, Cui K, Rodrigez J, Hu G, Zhang Z, Larson DR and Zhao K: CTCF-Mediated Enhancer-Promoter interaction is a critical regulator of Cell-to-Cell variation of gene expression. Mol Cell 67: 1049-1058.e6, 2017.
48. Kubo N, Ishii H, Xiong X, Bianco S, Meitinger F, Hu R, Hocker JD, Conte M, Gorkin D, Yu M, *et al*: Promoter-proximal CTCF binding promotes distal enhancer-dependent gene activation. Nat Struct Mol Biol 28: 152-161, 2021.
49. Llovet JM, Kelley RK, Villanueva A, Singal AG, Pikarsky E, Roayaie S, Lencioni R, Koike K, Zucman-Rossi J and Finn RS: Hepatocellular carcinoma. Nat Rev Dis Primers 7: 6, 2021.
50. Samanta A, Saha P, Johnson O, Bishayee A and Sinha D: Dysregulation of delta Np63 alpha in squamous cell carcinoma and its therapeutic targeting. Biochim Biophys Acta Rev Cancer 1879: 189034, 2024.
51. Li Y, Giovannini S, Wang T, Fang J, Li P, Shao C and Wang Y; TOR centre; Shi Y, Candi E, *et al*: p63: A crucial player in epithelial stemness regulation. Oncogene 42: 3371-3384, 2023.
52. Steurer S, Riemann C, Büscheck F, Luebke AM, Kluth M, Hube-Magg C, Hinsch A, Höflmayer D, Weidemann S, Fraune C, *et al*: p63 expression in human tumors and normal tissues: A tissue microarray study on 10,200 tumors. Biomark Res 9: 7, 2021.
53. Safri F, Nguyen R, Zerehpooshnesfchi S, George J and Qiao L: Heterogeneity of hepatocellular carcinoma: From mechanisms to clinical implications. Cancer Gene Ther 31: 1105-1112, 2024.
54. Deng J, Lai G, Zhang C, Li K, Zhu W, Xie B and Zhong X: A robust primary liver cancer subtype related to prognosis and drug response based on a multiple combined classifying strategy. Heliyon 10: e25570, 2024.
55. Gatti V, Fierro C, Annicchiarico-Petruzzelli M, Melino G and Peschiaroli A: ΔNp63 in squamous cell carcinoma: Defining the oncogenic routes affecting epigenetic landscape and tumour microenvironment. Mol Oncol 13: 981-1001, 2019.
56. Choi JH and Thung SN: Advances in histological and molecular classification of hepatocellular carcinoma. Biomedicines 11: 2582, 2023.
57. Qi W and Zhang Q: Insights on epithelial cells at the single-cell level in hepatocellular carcinoma prognosis and response to chemotherapy. Front Pharmacol 14: 1292831, 2023.
58. Gromowski T, Lukacs-Kornek V and Cisowski J: Current view of liver cancer cell-of-origin and proposed mechanisms precluding its proper determination. Cancer Cell Int 23: 3, 2023.
59. Fisher ML, Balinth S and Mills AA: p63-related signaling at a glance. J Cell Sci 133: jcs228015, 2020.
60. Kanchanawong P and Calderwood DA: Organization, dynamics and mechanoregulation of integrin-mediated cell-ECM adhesions. Nat Rev Mol Cell Biol 24: 142-161, 2023.
61. Chen Q, Guo H, Jiang H, Hu Z, Yang X, Yuan Z, Gao Y, Zhang G and Bai Y: S100A2 induces epithelial-mesenchymal transition and metastasis in pancreatic cancer by coordinating transforming growth factor β signaling in SMAD4-dependent manner. Cell Death Discov 9: 356, 2023.
62. Yang NY, Pasquale EB, Owen LB and Ethell IM: The EphB4 receptor-tyrosine kinase promotes the migration of melanoma cells through Rho-mediated actin cytoskeleton reorganization. J Biol Chem 281: 32574-32586, 2006.
63. Liu B, Feng Y, Xie N, Yang Y and Yang D: FERMT1 promotes cell migration and invasion in non-small cell lung cancer via regulating PKP3-mediated activation of p38 MAPK signaling. BMC Cancer 24: 58, 2024.
64. Guo K, Zhang J, Huang P, Xu Y, Pan W, Li K, Chen L, Luo L, Yu W, Chen S, *et al*: KANK1 shapes focal adhesions by orchestrating protein binding, mechanical force sensing, and phase separation. Cell Rep 42: 113321, 2023.
65. Zhao X, Wang E, Xu H and Zhang L: Stratifin promotes the growth and proliferation of hepatocellular carcinoma. Tissue Cell 82: 102080, 2023.
66. Brayer S, Joannes A, Jaillet M, Gregianin E, Mahmoudi S, Marchal Sommé J, Fabre A, Mordant P, Cazes A, Crestani B and Mailleux AA: The pro-apoptotic BAX protein influences cell growth and differentiation from the nucleus in healthy interphasic cells. Cell Cycle 16: 2108-2118, 2017.
67. He X, Ma Y, Huang Z, Wang G, Wang W, Zhang R, Guo G, Zhang X, Wen Y and Zhang L: SERPINB5 is a prognostic biomarker and promotes proliferation, metastasis and epithelial-mesenchymal transition (EMT) in lung adenocarcinoma. Thorac Cancer 14: 2275-2287, 2023.
68. Yao Y, Zhou D, Shi D, Zhang H, Zhan S, Shao X, Sun K, Sun L, Wu G, Tian K, *et al*: GLI1 overexpression promotes gastric cancer cell proliferation and migration and induces drug resistance by combining with the AKT-mTOR pathway. Biomed Pharmacother 111: 993-1004, 2019.
69. Gabriele M, Brandão HB, Grosse-Holz S, Jha A, Dailey GM, Cattoglio C, Hsieh TS, Mirny L, Zechner C and Hansen AS: Dynamics of CTCF- and cohesin-mediated chromatin looping revealed by live-cell imaging. Science 376: 496-501, 2022.
70. Liu Q, Jiang S, Xu X, Xu K, Luo Y, Yu Z, Xiang M, Xu Z, Wang L, Zhang S, *et al*: TP63 mediates the generation of tumour-specific chromatin loops that underlie MYC activation in radiation-induced tumorigenesis. Nat Commun 16: 8718, 2025.
71. Liu Y, Liu P, Duan S, Lin J, Qi W, Yu Z, Gao X, Sun X, Liu J, Lin J, *et al*: CTCF enhances pancreatic cancer progression via FLG-AS1-dependent epigenetic regulation and macrophage polarization. Cell Death Differ 32: 745-762, 2025.

Copyright © 2026 Lin et al. This work is licensed under a Creative Commons Attribution-NonCommercial-NoDerivatives 4.0 International (CC BY-NC-ND 4.0) License.